Concentration effects on segregation behavior of Pt-Rh nanoparticles

Koretaka Yuge

Department of Materials Science and Engineering, Kyoto University, Sakyo, Kyoto 606-8501, Japan

(Received 20 April 2011; revised manuscript received 4 July 2011; published 30 August 2011)

Based on the first-principles calculation combined with the cluster expansion technique and the Monte Carlo statistical simulation, concentration dependence of segregation behavior for Pt-Rh cuboctahedral nanoparticles is quantitatively examined. Several ground-state atomic arrangements for the nanoparticles at $T = 0$ K are predicted where Pt atoms prefer surface sites, particularly, at vertex sites with the lowest coordination number. We find strong Pt segregation at the surfaces of nanoparticles. Concentration dependence of segregation behavior for the nanoparticle is essentially different from that of the bulk Pt-Rh surface. Temperature dependence of segregation in the nanoparticles only appears for Pt composition at around 30%–70% due to the finite number of constituent atoms and to substantial Pt segregation at the surface. Warren-Cowley short-range-order parameters for vertex-edge and vertex-(100) pairs change their signs with respect to the Pt composition. This can be attributed to the significant Pt segregation at the vertex site, which should disrupt the tendency for the preference of unlike-atom pairs found at low Pt compositions. We find that the magnitude relationship of the Pt composition for surface sites is significantly affected by Pt composition in the nanoparticle.

DOI: 10.1103/PhysRevB.84.085451 PACS number(s): 81.30.−t, 64.70.kd

I. INTRODUCTION

It is expected that metal nanoparticles exhibit different properties from bulk, owing to finite-size effects and high surface-to-volume ratio, which motivate investigations for physical as well as chemical applications.[1–5] Extensive investigation and synthesis for bimetallic nanoparticles have actively been performed in recent years since alloying other elements can significantly modify catalytic properties. One of the well-investigated systems in experiments is the Pt-Rh nanoparticle because of its enhanced catalytic property including NO_x reduction, CO chemisorption, and hydrogenation.[6,7] So far, a wide variety of experiments synthesizes the Pt-Rh nanoparticles, such as those with colloid synthesis in polymer solutions using borohydride-reduction NaY-supported clusters using the ion-exchange method, pulsed laser ablation, and polyol synthesis.[1,6,8–13] Since the atomic structure and composition should significantly affect catalytic properties, understanding thermodynamic stability, including atomic structures and segregation behavior, should be a fundamental and significant prerequisite for the design of desirable alloy nanoparticles in terms of narrowing down the controlling parameters. Therefore, careful experimental studies on the size, the composition, and the structure of the Pt-Rh nanoparticle have been performed based on techniques, such as dispersive x-ray analysis, transmission electron microscope, extended x-ray absorption fine structure, and x-ray photoelectron spectroscopy. Diameters with 1–4-nm nanoparticles are typically synthesized, and their preferably segregated species as well as atomic arrangements depend on the sample preparation condition or method.

Theoretical studies based on density functional theory (DFT) for Pt and Rh metal nanoparticles have also been performed to investigate stable atomic arrangements:[14–20] A number of stable or metastable metal nanoparticles, consisting of up to $\sim$300 atoms, are extensively studied with icosahedron, cuboctahedron, octahedron, biplanar, and lower-symmetry shapes, while their relative stability is still under discussion. Pt and Rh nanoparticles with cuboctahedral and icosahedral shapes particularly have been considered interesting since they are linked to each other through Mackay transformation with small energy differences, and they are Platonic and Archimedean solids in uniform polyhedra.[15]

In contrast to such extensive studies on Pt and Rh nanoparticles, theoretical studies on the segregation behavior for the Pt-Rh nanoparticle somehow have been confined to the empirical method including the pair-bond energy model[21] and free-energy concentration expansion[22] where the dependence of energies on atomic arrangements is described by the empirical formula and their parameters are determined based on experimental data: These studies predict Pt atoms energetically prefer to segregate at the surface rather than at the subsurfaces. Meanwhile, for other alloy nanoparticles, such as the Fe-Pt system, segregation behavior is quantitatively examined based on the tight-binding model[23] or the combination of first-principles calculations with the local cluster expansion (CE) technique.[24] Very recently, based on DFT calculations combined with the CE technique, we quantitatively investigated the segregation behavior of equiatomic $Pt_{28}Rh_{27}$ cuboctahedral nanoparticles.[25,26] We found that Pt atoms tended to segregate at surface sites due to a large difference in on-site energy, which is a segregation tendency similar to the bulk Pt-Rh surface.[27] We also find that, unlike the bulk surface, an ordering tendency is more essential to describe preferable segregation of particular edge and (100) sites at the surfaces of nanoparticles. Another important point, specific to nanoparticles, is the concentration dependence of segregation behavior. For a bulk Pt-Rh alloy surface, Pt atoms tend to segregate at the topmost layer, and Rh atoms tend to segregate at the subsurface for the whole composition. Meanwhile, since the nanoparticle itself does not equilibrate to an infinite bulk reservoir, its concentration dependence of segregation does not necessarily follow the bulk. With these considerations, theoretical assessment on the concentration dependence of segregation behavior through DFT calculation is highly desirable in order to investigate segregation, specific to alloy nanoparticles. In the present paper, we concentrate

on the study of a Pt-Rh nanoparticle consisting of 55 atoms with a cuboctahedron shape. We have combined the first-principles calculation with the CE technique[28,29] and Monte Carlo (MC) statistical simulations in order to quantitatively investigate energetic stability, ground-state structures, and the segregation behavior, including the ordering effects of the Pt-Rh nanoparticles in various Pt compositions.

II. METHODOLOGY

We employ the CE technique to express DFT energies for Pt-Rh nanoparticles in terms of their composition and atomic arrangements. In the case of CE for the nanoparticle, we have five symmetry-nonequivalent sites of the vertex, edge, (100), subsurface, and core as shown in Fig. 1. The details of the present CE approach are essentially the same as described in our previous papers:[26,30] Two basis functions of σ and 1 (unity) at each lattice point are used to construct complete and orthonormal basis functions, where $\sigma_i = +1$ represents Pt occupation at site i and $\sigma_i = -1$ represents Rh occupation in the present paper. In order to construct a 55-atom cuboctahedral nanoparticle, we first construct a supercell, which is obtained by expanding $5 \times 5 \times 5$ of a fcc unit cell. Then, atoms that do not belong to the nanoparticle are excluded from the supercell. Subsequently, the resultant cell gives initial positions for the 55-atom nanoparticle whose atomic positions are optimized in the DFT calculation to reduce forces acting on the individual atoms. We employ first-principles calculations using a DFT code, the Vienna *ab initio* simulation package,[31,32] to obtain total energies for ordered structures that are least-squares fitted to the CE Hamiltonian to determine the expansion coefficients in the CE, i.e., effective cluster interactions (ECIs). The ordered structures consist of 327 Pt_nRh_{55-n} nanoparticles, where n takes 4, 12, 20, 28, 36, 44, and 52. The other calculation condition for the first-principles calculations is the one according to our previous paper.[26]

Since there is a limitation on the number of DFT input energies, finite numbers of clusters that are optimal for describing the system of interests should be selected. Details of how to select clusters and structures are described in our previous papers:[33–35] In brief terms, we employ a genetic algorithm in order to minimize the uncertainty of energies predicted by the ECIs, which is called a cross-validation (CV) score.[36,37] DFT input structures are chosen based on a ground-state diagram[38] so that resultant ECIs can predict energies not only for energetically favored ordered structures but also for high-energy structures in order to precisely treat ground-state-ordered structures as well as disordered structures at high temperatures.

We apply ECIs for the optimal set of clusters to a MC simulation under a canonical ensemble using the Metropolis algorithm. In order to obtain ground-state atomic arrangements at $T = 0$ K, a simulated annealing algorithm was employed. Starting at 3000 K, the temperature of the simulation box, subsequently, was decreased by 20 K after 4000 MC steps per site. At finite temperatures, 15 000 MC steps per site were performed for equilibration, followed by 4000 MC steps per atom for sampling at each temperature and composition. In each MC step, the total energies of the system, atomic position, and correlation functions were stored.

III. RESULTS AND DISCUSSION

A. Multibody effective interactions for the Pt-Rh nanoparticle

Thirty-seven optimal clusters are selected following the procedure described in Sec. II, which consists of one empty, five point, nineteen pair, nine triplet, and three quadruplet clusters. Here, we note that, although four of five point clusters are selected for the $Pt_{28}Rh_{27}$ nanoparticle, all five point clusters are selected for the Pt-Rh nanoparticle since the five clusters are linearly independent due to considering a variety of compositions. Another notation is that the selected set of 37 clusters is different from that used for $Pt_{28}Rh_{27}$ nanoparticles obtained in our previous paper. This is because the present paper includes a variety of Pt compositions, including $Pt_{28}Rh_{27}$. Therefore, a set of DFT input structures for CE in the present case differs from the previous case of $Pt_{28}Rh_{27}$, which leads to a different interpretation of effective interactions and should lead to a different set of clusters that is optimal to describe energies for compositions of interest. At the equiatomic composition of $Pt_{28}Rh_{27}$, we confirm that ECIs obtained through whole composition in the present paper successfully predict the same ground-state structure as predicted by ECIs obtained through a fixed composition of $Pt_{28}Rh_{27}$ in our previous paper.[26] In Fig. 2, multibody clusters are illustrated by dark spheres connected with bold lines. In each dimension and type of cluster, the cluster numbers are assigned so that clusters close to the core have the larger numbers as much as possible.

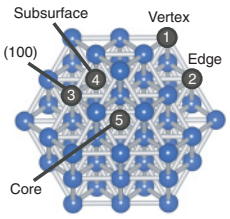

FIG. 1. (Color online) Symmetry-nonequivalent sites of the vertex, edge, (100), subsurface, and core of the Pt-Rh nanoparticle are represented by black spheres.

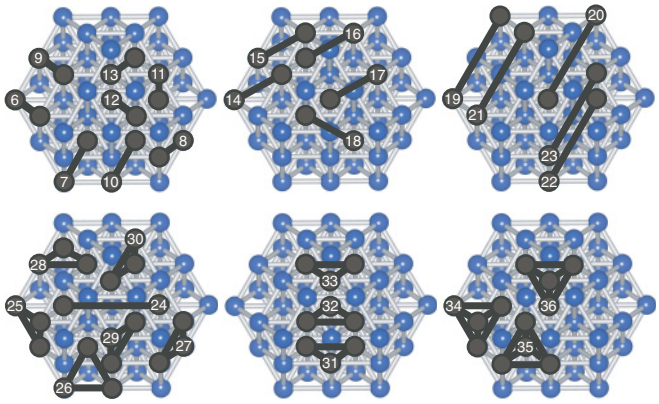

FIG. 2. (Color online) Selected multibody clusters used in the expansion of the total energies for the Pt-Rh bimetallic nanoparticle. Dark spheres connected with bold lines represent used clusters.

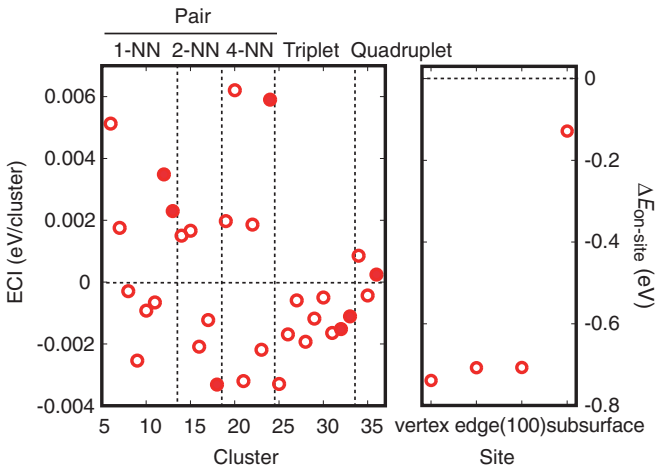

FIG. 3. (Color online) (Left) ECIs for multibody clusters. Closed circles correspond to clusters consisting of subsurface and/or core sites, and open circles correspond to other clusters. (Right) Pt on-site energy measured from that of the core site, defined by $2(V^{(1)} - V^{(1)}_{\text{core}})$.

The pair clusters consist of first-nearest-neighbor (1-NN) (Nos. 6–13 in Fig. 2), second-nearest-neighbor (2-NN) (Nos. 14–18), and fourth-nearest-neighbor (Nos. 19–24) clusters. The triplet and quadruplet clusters (Nos. 25–33 and Nos. 34–36, respectively) all consist of 1-NN pairs. These selected clusters give a CV score of 2.9 meV/atom, which is sufficient to express the relative energies of the ordered structures for the Pt-Rh nanoparticle.

On the left-hand side of Fig. 3, ECIs for multibody clusters are shown in terms of the cluster figure. Closed circles denote ECIs for clusters consisting of subsurface and/or core sites, and open circles denote those for other clusters. We clearly can see that dominant contributions to the total energy of the Pt-Rh nanoparticle come from ECIs for pair clusters. ECIs for surface sites have a wide variety of values, which depend on the position of their clusters, indicating that the ordering tendency is anisotropic for inner shells and surfaces.

B. Segregation tendency in terms of on-site energy

According to our previous paper on the bulk Pt-Rh alloy and on the $Pt_{28}Rh_{27}$ nanoparticle, the dominant contribution to surface segregation comes from Pt on-site energy. Therefore, segregation behavior can be predicted qualitatively in terms of the on-site energy measured from that at the core site, which can be described in the CE approach by the difference in twice the ECI for point clusters between site I and core site $\Delta E^{\text{I}}_{\text{on-site}} = 2(v^{(1)}_{\text{I}} - v^{(1)}_{\text{core}})$. Here, $\Delta E^{\text{I}}_{\text{on-site}} < 0$ denotes that Pt atoms energetically prefer site I rather than the core site in terms of point ECIs, and $\Delta E^{\text{I}}_{\text{on-site}} > 0$ denotes the opposite. On the right-hand side of Fig. 3, we show the calculated $\Delta E^{\text{I}}_{\text{on-site}}$ for vertex, edge, (100), and subsurface sites. All the on-site energies exhibit a negative sign, which indicates that the Pt atom energetically disfavors the core site and favors the outer shell of the nanoparticle. Particularly, the on-site energies of the three sites at the surface are significantly larger when they have a negative sign than that for the subsurface, indicating a strong Pt segregation at the surface. However, differences in on-site energies among vertex, edge, and (100) sites are on the same order as the ECIs for multibody clusters on the left-hand side of Fig. 3. This fact certainly indicates that preferable Pt segregation sites at the surface can be affected significantly by multibody interactions, which hold, particularly, for segregation at the edge and (100) sites where no practical difference can exist in the on-site energy between these two sites.

C. Quantitative estimation of segregation behavior

Before proceeding to quantitative segregation behavior, it can be useful to start with a discussion about ground-state atomic arrangements at $T = 0$ K, which typically link with segregation at finite temperatures. We predict ground-state atomic arrangements at $T = 0$ K for $Pt_{20}Rh_{35}$, $Pt_{28}Rh_{27}$, and $Pt_{36}Rh_{19}$ nanoparticles as shown in Fig. 4. Dark spheres denote Pt atoms, and bright spheres denote Rh atoms. At lower compositions of $Pt_{20}Rh_{35}$, all 12 vertex sites are occupied by Pt atoms, and the other eight Pt atoms all occupy edge sites. This can be attributed to the lower total energy of the Pt_1Rh_{54} nanoparticle with a single Pt atom at the vertex and edge sites.[25] At higher compositions of $Pt_{36}Rh_{19}$, all 12 vertex sites are similarly occupied by Pt atoms, while edge sites are partially occupied by Pt atoms (18 sites out of 24), and all six (100) sites are occupied by Pt atoms. From these ground-state atomic arrangements, substantial Pt segregation at the surface, particularly at vertex sites, is predicted. Here, we should note that interpretation of the ground state for nanoparticles is essentially different from that for bulk. For bulk, ground-state diagrams determine phase separation for intermediate composition with no structures on ground-state lines. Meanwhile, since nanoparticles themselves do not actually exchange atoms with each other, energetically stable atomic arrangements are determined not by the ground-state line, but by the ground state at corresponding compositions. Therefore, in terms of the synthesis of alloy nanoparticles, ground states for individual compositions would all be significantly informative.

Next, using a combination of on-site energy and multibody cluster ECIs with MC simulation as described in Sec. II, we quantitatively estimate segregation behavior of the Pt-Rh nanoparticle at finite temperatures. Figure 5 shows the segregation behavior at $T = 100$ and 1300 K in terms of Pt composition at five symmetry-nonequivalent sites as a function of Pt composition in the Pt-Rh nanoparticle. We can find strong Pt segregation at the vertex sites for whole Pt composition in the Pt-Rh nanoparticle at both high and low temperatures. Due to the strong Pt segregation at the

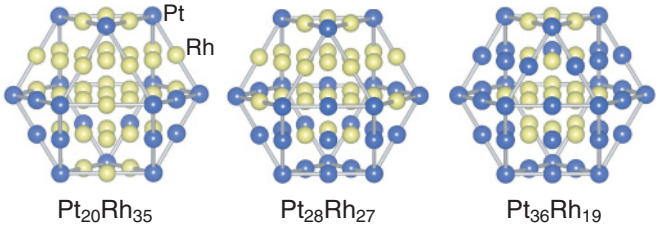

FIG. 4. (Color online) Predicted ground-state atomic configurations for $Pt_{20}R_{35}$, $Pt_{28}Rh_{27}$, and $Pt_{36}Rh_{19}$. Dark spheres denote Pt atoms, and bright spheres denote Rh atoms.

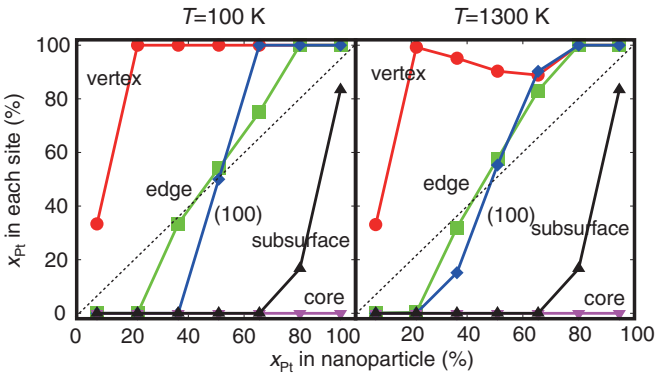

FIG. 5. (Color online) Pt composition at five symmetry-nonequivalent sites as a function of Pt composition in the Pt-Rh nanoparticle at $T = 100$ and 1300 K.

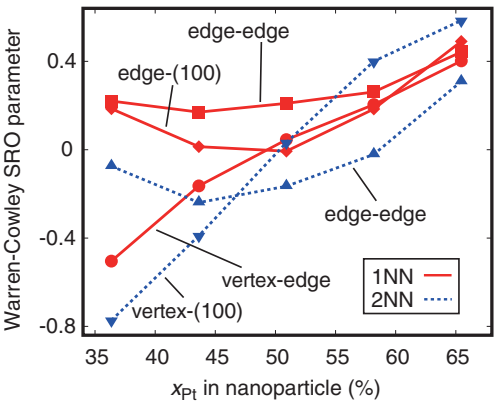

FIG. 6. (Color online) Calculated Warren-Cowley SRO parameters for pairs in the 1-NN and 2-NN as a function of Pt composition in the Pt-Rh nanoparticle at $T = 1300$ K.

vertex sites, the segregation profile of the Pt-Rh nanoparticle at $T = 1300$ K is significantly different from that of the bulk Pt-Rh surface with Pt enrichment at the surface and Pt depletion at the subsurface for the whole composition. The result of preference at the edge site compared with the (100) site for lower Pt composition can be attributed to lower total energy of the Pt_1Rh_{54} nanoparticle with a single Pt atom at edge sites than that at (100) sites. Pt composition at the subsurface and core do not depend on temperature. This should reflect a large energy gain for Pt segregation at the subsurface and core with respect to sites at the surface. Comparing the segregation profile at $T = 1300$ K with that at $T = 100$ K in Fig. 5, we find that dependence of Pt segregation on temperature appears for limited Pt composition of around 30%–70%, which would be attributed to substantial Pt segregation at the surface and to a finite number of constituent atoms in the nanoparticles.

Finally, in order to see which type of atomic pairs (i.e., like- or unlike-atom pairs) are preferred at the surface of the Pt-Rh nanoparticle, we estimate the Warren-Cowley short-range order (SRO) parameter[39] α. Here, $\alpha < 0$ indicates the preference of the Pt-Rh pairs in terms of the disordered state, and $\alpha > 0$ denotes disfavor of the Pt-Rh pairs. Figure 6 shows calculated SRO parameter α for 1-NN and 2-NN pairs at the surface as a function of composition where temperature dependence of segregation can be seen. α for 1-NN vertex-edge pairs and 2-NN vertex-(100) pairs exhibits a similar composition dependence: At low Pt compositions, α has large negative values, which increase with an increase in Pt composition, and it has positive values at high Pt compositions. When Pt composition increases, Pt compositions of vertex, edge, and (100) sites exceed the Pt composition of the nanoparticle itself. Such strong Pt segregation at the surface certainly disrupts the preference of the Pt-Rh pairs and significantly increases Pt-Pt like-atom pairs, which should lead to an increase in α for the two pairs. This tendency also holds for α for 2-NN edge-edge pairs: α exhibits a negative sign at lower Pt composition, while at higher Pt composition, α displays a positive sign. α for 1-NN edge-(100) and edge-edge pairs exhibits a positive sign for the whole composition range, indicating a preference of like-atom pairs. These results indicate that, at lower Pt compositions, the preference for the Pt-Rh pairs is retained at the surface, while at higher Pt compositions, the preference of the Pt-Rh pairs is significantly diminished due to strong Pt segregation at the surface.

IV. CONCLUSION

Concentration dependence of segregation behavior for the Pt-Rh nanoparticles is systematically investigated through the first-principles calculations combined with the CE technique and MC statistical simulation. We predict several ground-state atomic arrangements of the Pt-Rh nanoparticles at $T = 0$ K, where Pt atoms tend to locate at surface sites as much as possible, particularly, at the vertex site with the lowest coordination number. We find strong Pt segregation at the surface of the Pt-Rh nanoparticle. Temperature dependence of Pt segregation only appears for intermediate Pt composition of around 30%–70% due to the finite number of constituent atoms and strong Pt segregation at the surface sites. At high Pt concentrations, the preference of unlike-atom pairs at the surface is significantly diminished due to the strong Pt segregation at the vertex sites. For edge and (100) sites, the preference of Pt segregation depends on Pt composition: At low Pt compositions, Pt prefers edge sites, while at high Pt compositions, Pt prefers (100) sites.

ACKNOWLEDGMENTS

This research was supported by a Grant-in-Aid for Young Scientists B (Grant No. 22760502) by JSPS.

[1]N. Toshima and T. Yonezawa, New J. Chem. **1**, 1179 (1998).
[2]M. Valden, X. Lai, and D. W. Goodman, Science **281**, 1647 (1998).
[3]J. Meier, K. A. Friedrich, and U. Stimming, Faraday Discuss. **121**, 365 (2002).
[4]N. Lopez and J. K. Norskov, J. Am. Chem. Soc. **124**, 11262 (2002).
[5]F. Maillard, M. Eikerling, O. V. Cherstiouk, S. Schreier, E. Savinova, and U. Stimming, Faraday Discuss. **125**, 357 (2004).

[6]K. Siepen, H. Bönnemann, W. Brijoux, J. Rothe, and J. Hormes, Appl. Organometal. Chem. **14**, 549 (2000).
[7]C. E. Lyman, R. E. Lakis, and H. G. Stenger, Ultramicroscopy **58**, 25 (1995).
[8]N. Savastenko, H. R. Volpp, O. Gerlach, and W. Strehlau, J. Nanopart. Res. **10**, 277 (2008).
[9]Y. Wang, J. Zhang, X. Wang, J. Ren, B. Zuo, and Y. Tang, Topics Catal. **35**, 35 (2005).
[10]M. Harada, K. Asakura, and N. Toshima, J. Phys. Chem. **98**, 2653 (1994).
[11]T. Hashimoto, K. Saijo, M. Harada, and N. Toshima, J. Phys. Chem. **109**, 5627 (1998).
[12]M. Harada and H. Einaga, J. Colloid Interface Sci. **308**, 568 (2007).
[13]E. Cimini and R. Prins, J. Phys. Chem. B **101**, 5285 (1997).
[14]S. K. Nayak, S. E. Weber, P. Jena, K. Wildberger, R. Zeller, P. H. Dederichs, V. S. Stepanyuk, and W. Hergert, Phys. Rev. B **56**, 8849 (1997).
[15]C. Barreteau, M. C. Desjonquëres, and D. Spanjaard, Eur. Phys. J. D **11**, 395 (2000).
[16]L. Wang and Q. Ge, Chem. Phys. Lett. **366**, 368 (2002).
[17]V. Kumar and Y. Kawazoe, Eur. Phys. J. D **24**, 81 (2003).
[18]E. Aprà and A. Fortunelli, J. Phys. Chem. **107**, 2934 (2003).
[19]L.-L. Wang and D. D. Johnson, Phys. Rev. B **75**, 235405 (2007).
[20]V. Kumar and Y. Kawazoe, Phys. Rev. B **77**, 205418 (2008).
[21]A. de Sarkar and B. C. Khanra, Chem. Phys. Lett. **353**, 426 (2002).
[22]R. Vardi, L. Rubinovich, and M. Polak, Surf. Sci. **602**, 1040 (2008).
[23]B. Yang, M. Asta, O. N. Mryasov, T. J. Klemmer, and R. W. Chantrell, Scr. Mater. **53**, 417 (2005).
[24]R. V. Chepulskii, W. H. Butler, A. van de Walle, and S. Curtarolo, Scr. Mater. **62**, 179 (2010).
[25]K. Yuge, T. Ichikawa, and J. Kawai, Mater. Trans. **51**, 321 (2010).
[26]K. Yuge, J. Phys.: Condens. Matter **22**, 245401 (2010).
[27]K. Yuge, A. Seko, A. Kuwabara, F. Oba, and I. Tanaka, Phys. Rev. B **74**, 174202 (2006).
[28]J. M. Sanchez, F. Ducastelle, and D. Gratias, Physica A **128**, 334 (1984).
[29]J. M. Sanchez, Phys. Rev. B **48**, 14013 (1993).
[30]K. Yuge, A. Seko, A. Kuwabara, F. Oba, and I. Tanaka, Phys. Rev. B **76**, 045407 (2007).
[31]G. Kresse and J. Hafner, Phys. Rev. B **47**, R558 (1993).
[32]G. Kresse and J. Furthmüller, Phys. Rev. B **54**, 11169 (1996).
[33]K. Yuge, A. Seko, Y. Koyama, F. Oba, and I. Tanaka, Phys. Rev. B **77**, 094121 (2008).
[34]K. Yuge, J. Phys.: Condens. Matter **21**, 415401 (2009).
[35]K. Yuge, Phys. Rev. B **79**, 144109 (2009).
[36]M. Stone, J. R. Stat. Soc. Ser. B **36**, 111 (1974).
[37]D. M. Allen, Technometrics **16**, 125 (1974).
[38]V. Blum and A. Zunger, Phys. Rev. B **70**, 155108 (2004).
[39]J. M. Cowley, J. Appl. Phys. **21**, 24 (1950).